Supporting Online Material for "Genetic reactivation of cone photoreceptors restores complex visual responses in *Retinitis pigmentosa*" (Manuscript number: 1190897)

This file includes:

Supplementary Discussion

Selecting patients for possible eNpHR-based gene therapy.

Possible criteria to stratify patients for eNpHR-based therapy include the following: No central visual field in Goldmann perimetry; legal blindness; and no visible outer segments on OCT pictures; but a layer of cone cells in the foveal region at least. There may, however, be several other factors for consideration when selecting patients. First, after losing central vision it is most often difficult to obtain good quality OCT due to the lack of fixation. Improved OCT imaging techniques (*S1*) or, alternatively, a reversible blockade of muscle activity could overcome this difficulty. Second, the disappearance of the photoreceptor nuclear layer on OCT images is not necessarily indicative of complete photoreceptor loss: We found in the f-RD mouse model that, during the later stages, the AAV-labeled cone cells did not form a distinct layer above the outer plexiform layer, but merged into the upper row of the inner nuclear layer. In *Retinitis pigmentosa* patients, even at late stages, the macula has a monolayer of cone cell bodies (*S2*), which may not be detectable with current OCTs. New, high resolution and fast scanning techniques (*S1*) may facilitate the detection of even a single layer of cone cell bodies for eNpHR treatment. Third, we note that a major advantage of targeting remaining cone cell bodies with eNpHR, as compared with targeting bipolar or ganglion cells with channelrhodopsin (*S3, S4*), is that, unlike cones, bipolar and ganglion cells are not arranged in a mosaic in the fovea (since these cells are moved away from the path of light in the fovea) and, therefore, light stimulation with patterns will cause spatially irregular activation of bipolar and ganglion cells. Fourth, we noted both in the transgenic mice expressing NpHR on a wild-type background, and also in eNpHR-EYFP-AAV-injected wild-type mice, that normal visual function was preserved in these mice, and eNpHR induced additional light sensitivity at longer wavelengths. This

finding implies that it may even be beneficial to consider targeting cones with eNpHR in patients who have not completely lost central vision (*S5*). Since eNpHR is less sensitive than normal cones, stimulation will require image intensifier goggles (see below), and we predict that in the absence of these goggles the remaining natural vision will not be affected. This latter approach should only be considered if clinical results with patients with no central vision are established and safety is proved.

Light intensity requirements for eNpHR-based treatment

Since eNpHR-expressing cells are not able to adapt to different intensities, stimulator goggles with an adaptive front sensor array and an LED array (*S6, S7*) (or other patterned light source) facing the eye will be needed, independent of the exact sensitivity range of these halobacterial sensors. Without the goggles, halorhodopsins will not respond if the mean light intensity is too low, or halorhodopsins will be saturated if the mean light intensity is too high. The key point is that the sensitivity of halorhodopsins must be tuned to intensities that are safe for use in the human eye. In this respect, the red-shifted spectra of halorhodopsins (peak at 580nm) compared to that of channelrhodopsin (peak at 470 nm, blue light) is of importance, since blue light has a higher potential for inducing photochemical damage than yellow light (*S6*) We envision that adaptation to the different background intensities of the visual world will be achieved by artificial image sensors in the goggles, similar to those used in commercial video cameras. Nevertheless, new mutants and other types of light-activated ion pumps (*S8*) that produce more current per captured photon can make it even more sure that the light intensity required to stimulate the eye is safe (*S6*). There are two factors that may be worth balancing for potential clinical trials. On the one hand, increasing the sensitivity of eNpHR-transduced cones, by enhanced expression of eNpHR or by increased current per photon, is beneficial for safe stimulation.

On the other hand, the sensitivity should not be too high: If the regained visual sensation may, for some unforeseen reason, cause headache or tiredness after long light exposure, eNpHR stimulation could be turned off by removing the stimulation goggles. Finally, light-sensitive pumps activated at different wavelengths (*S8*) may open the way for restoring color vision.

The state of cone photoreceptors in RD mice.

Cones of healthy retinas respond to light with hyperpolarization caused by the closure of cyclic-nucleotide gated (CNG) channels (*S9*) located in the cone outer segment. CNG channels are open in the dark, and their closure is controlled through a molecular cascade induced by the capture of photons by opsins. In later stages of RD, the outer segment of cones degenerate and, therefore, one would expect no dark current and, consequently, a hyperpolarized cone. In contrast, we found that RD cone cell bodies were depolarized at −26 mV. Although the reason for the depolarized state is currently not understood, we speculate here about a mechanism. One possibility is that CNG channels in RD retinas are present in the remaining cone cell body but these channels are no longer modulated by opsins. However, this explanation is inadequate because the CNG channels are not functional (Cnga3-/-) in s-RD mice, and CNG channel expression is low in f-RD mice (see Fig. S5). There are at least three other potential mechanisms. First, a compensatory mechanism may exist at the level of gene regulation that induces the expression of genes that keep the cell body in a depolarized state, for example by up-regulation of constitutively open Na^+, Ca^{2+}, or nonselective ion channels, either alone or in combination with the down-regulation of K^+ or Cl^- channels. Second, depolarization can be achieved by a ligand, present in RD but not wild type retinas, that opens Na^+, Ca^{2+}, or nonselective ion channels or closes K^+ or Cl^- channels. Third, it is possible that the ion concentrations in the cone

change in RD in such a way that a channel, for example a Cl^- channel, may have a new driving force. This last possibility alone is unlikely, since we controlled the ion concentrations in the recorded cone in our experiments. Finally, it is possible that the combination of these above events led to the depolarized state.

Materials and methods

Plasmids. The sources and names of the plasmids that were used as starting materials are listed in Supplementary Table S2. Restriction enzymes were purchased from New England Biolabs. Polymerase chain reaction (PCR)-based cloning was performed using Herculase polymerase (Stratagene) followed by sequencing to verify that the constructs were free of mutations. The In-Fusion 2.0 PCR Cloning Kit (Clontech) was used to insert PCR products into linearized plasmids via homologous recombination. Primers for In-Fusion cloning were designed to comprise 21 bp homology to the PCR product and 15 bp homology to the target vector backbone. In some cloning steps, linearization was performed using two restriction enzymes to remove unwanted DNA segments.

First, to obtain pAAV2-hRHO-eNpHR-EYFP we linearized pAAV2.1-Rho-EGFP using NotI/HindIII, and inserted the PCR-amplified eNpHR-EYFP from Lenti-CaMKIIa-eNpHR-EYFP-WPRE (*S10*). Forward primer: atcacactggcggccctagcgccaccatgaggggta. Reverse primer: gattggatccaagcttcattacacctcgttctcgta. Note that Rho in pAAV2.1-Rho-EGFP and hRHO refer to the same promoter (hRHO, 0.9 kb).

Second, to obtain pAAV2-hRO-EGFP we linearized pAAV2.1-Rho-EGFP using NheI/NotI and inserted the PCR-amplified human red opsin promoter (hRO, 2.1 kb) from

pRed2.1lacZ (*S11*). Forward primer: tcgcccttaagctagcctacagcagccagggtgaga. Reverse primer: cgcccttgctcaccatggcggccgctatggaaagcc.

Third, to obtain pAAV2-hRO-eNpHR-EYFP we linearized pAAV2-hRO-EGFP using NotI/HindIII and inserted the PCR-amplified eNpHR-EYFP from Lenti-CaMKIIa-eNpHR-EYFP-WPRE. Forward primer: ctttccatagcggcctgccaccatgaggggtacgcc. Reverse primer: attggatccaagctattacacctcgttctcgtagca.

Fourth, to generate the intermediate plasmid pCR-Blunt II-TOPO-mCAR, the mouse cone arrestin promoter fragment (*S12*) (mCAR, 0.5 kb) upstream of the Arr3 gene was PCR-amplified from mouse genomic DNA. Forward primer: ggttcttcccattttggcta. Reverse primer: cctccagctctggttgctaag. mCAR was then subcloned into the pCR-Blunt II-TOPO (Invitrogen) vector backbone. To obtain pAAV2-mCAR-EGFP, we linearized pAAV2.1-Rho-EGFP using NheI/EcoRV and inserted the PCR-amplified mCAR from pCR-Blunt II-TOPO-mCAR. Forward primer: tcgcccttaagctagggttcttcccattttggctac. Reverse primer: gccagtgtgatggatcctccagctctggttgctaag.

Fifth, to obtain pAAV2-mCAR-eNpHR-EYFP we linearized pAAV2-mCAR-EGFP using NotI/HindIII and inserted the PCR-amplified eNpHR-EYFP from Lenti-CaMKIIa-eNpHR-EYFP-WPRE. Forward primer: atcacactggcggcctgccaccatgaggggtacgcc. Reverse primer: attggatccaagctattacacctcgttctcgtagca.

Sixth, to obtain pLV-mCAR-eNpHR-EYFP we linearized pRRLsincPPT-hPGK using EcoRV/BamHI and inserted the PCR-amplified mCAR-eNpHR-EYFP from pAAV2-mCAR-eNpHR-EYFP. Forward primer: ctcgagaagcttgatggttcttcccattttggctac. Reverse primer: ctgtttaaacggatcctattacacctcgttctcgta.

Seventh, to obtain pbRHO-NpHR-EYFP (here bRho refers to the bovine rhodopsin promoter, 2.2 kb) the pRho-DsRed (*S13*) was linearized using KpnI/NotI. The NotI site was blunted using T4 polymerase (New England Biolabs). NpHR-EYFP was cut out of pcDNA3.1/NpHR-EYFP (*S14*) using KpnI/XbaI. The XbaI site was blunted using T4 polymerase. The two DNA fragments were ligated (2x Mighty Ligation Mix, Takara Bio) and called pbRHO-NpHR-EYFP. pbRHO-NpHR-EYFP was used for pronuclear injections to obtain transgenic mice in FVB background.

Eighth, to obtain pAAV2-hRHO-NpHR-EYFP we cut out NpHR-EYFP from pcDNA3.1/NpHR-EYFP (*S14*) using NheI/BsrGI. The NheI site was blunted and NpHR-EYFP was ligated to EcoRV/BsrGI linearized pAAV2.1-Rho-EGFP (2x Mighty Ligation Mix, Takara Bio).

Animals. Wild-type C57BL/6 mice were purchased from RCC Ltd. (Füllinsdorf, Switzerland). C3H/HeNCrl (*Pde6b*^{rd1}) mice were purchased from Charles River Laboratories (L'Arbresle Cedex, France). *Cnga3*$^{-/-}$; *Rho*$^{-/-}$ double knockout mice were provided by Mathias Seeliger, Peter Humphries, and Martin Biel. The Fvb-Rho-NpHR-EYFP mouse line was generated in the transgenic mouse production facility at the Friedrich Miescher Institute. For this study, it was backcrossed to C57BL/6 mice. All animal experiments and procedures were approved by the Swiss Veterinary Office. The animals were maintained under a 12-hour light-dark cycle. The age ranges of mice used for particular experiments are listed in Supplementary Table S1. The ages of mice transfected with AAVs and used for retinal electrophysiology are shown in Fig. S7.

AAV production. All recombinant adeno-associated viruses were made by Penn Vector Core and serotyped as listed in Supplementary Table S3. Penn Vector Core performed the

genome copy (GC) number titration (see Supplementary Table S3) by using real-time PCR (TaqMan reagents, Applied Biosystems).

Lentivirus production. Lentivirus was produced as previously described (*S15*). The titer of LV-mCAR-eNpHR-EYFP was 2×10^9 VG/ml (viral genomes per ml).

Subretinal AAV administration. The animals were anaesthetized using 3% isoflurane. A small incision was made with a sharp 30-gauge needle in the sclera near the lens. Through this hole, 2µl AAV were injected slowly (in 20-30 s) into the subretinal space using a blunt 5 µl Hamilton syringe held in a micromanipulator. Mice older than P21 were used for injections. There was a minimum incubation time of 21 days before performing experiments on AAV-injected animals. For behavioral studies, we injected both eyes with either eNpHR- or EGFP-expressing AAVs.

Immunohistochemistry. Retinas were isolated and fixed in 4% paraformaldehyde in phosphate-buffered saline (PBS) for a maximum of 30 min at room temperature (RT), and washed in PBS overnight at 4°C. Retinal whole mounts were incubated in 30% sucrose overnight at RT. The retinas were treated with three freeze-thaw cycles. After the freeze-thaw treatment, all the steps were performed at RT. Retinas were incubated in a blocking solution (10% normal donkey serum (NDS, Chemicon), 1% bovine serum albumin (BSA), and 0.5% Triton X-100 in PBS, pH 7.4) for 1h. Primary and secondary antibody applications were done in 3% NDS, 1% BSA, 0.02% sodium azide, and 0.5% Triton X-100 in PBS. All antibodies, dilutions, and sources are listed in Supplementary Table S4. Primary antibodies were applied for 3-7 days. After washing the retina three times for 10 min in PBS, the retina was incubated with Alexa Fluor-conjugated secondary antibodies (1:200 dilution) and 10 µg/ml 4', 6-diamidino-2-phenylindole (DAPI, Roche Diagnostics),

which stains cell nuclei, for 2h. After another three washes in PBS, the retina was mounted on a glass slide with ProLong Gold antifade reagent (Invitrogen). Retinal vibratome sections: Fixed retinas were embedded in 3% agarose (SeaKem Le Agarose, Lonza) in PBS, and 150μm vertical sections were cut using a Leica VT1000S vibratome. Antibody staining procedure was the same as in whole mounts. Note that we used primary anti green fluorescent protein (GFP) antibodies to label EYFP because of epitope homology. Neurobiotin-filled ganglion cells from patch clamping experiments were stained with Alexa Fluor 555-conjugated streptavidin (Invitrogen) as previously described (*S16*). We used choline acetyl transferase antibody to mark two IPL strata (*S16*).

Confocal microscopy. Confocal images of antibody-stained retinas were taken using a Zeiss LSM 510 Meta Axioplan 2 laser scanning confocal microscope (Carl Zeiss) equipped with argon and helium-neon lasers. Plan-Apochromat 63x/1.4 or 40x/1.4 oil immersion objective lenses were used. Image analysis and quantification were done using Imaris software (Bitplane).

Quantification of AAV transduction. At least three retinal whole mounts per mouse line and AAV type were immunostained for GFP (to label eNpHR-EYFP- or EGFP-expressing cells) and cone arrestin (to label cones), as well as stained with DAPI (to label cell nuclei in order to count the total number of photoreceptors). In each wild-type retina the entire depth of the ONL was scanned by confocal microscopy at three randomly-chosen areas in AAV-transduced regions. Three horizontal sections of each ONL scan (top layer, central layer, and bottom layer close to OPL) were analyzed. Automatic cell count in Imaris (Bitplane) was used to determine the number of GFP-labeled, cone-arrestin-labeled, and DAPI positive photoreceptors. Because eNpHR-EYFP is membrane-bound, the GFP channel in eNpHR-EYFP-transduced retinas was inverted. This inversion enabled automatic cell

counting. After this automatic cell count procedure, which marked every counted cell, each confocal section was manually inspected to remove false automatic counts. In RD retinas the procedure was the same, but due to decreased ONL thickness only one horizontal section was analyzed per confocal scan. In total, 81 horizontal sections were analyzed from AAV-transduced wild-type retinas (n=7403 cells (hRHO), n=7974 (hRO), n=7996 (mCAR)), 26 for s-RD (n=1634 (hRHO), n=1865 (hRO), n=1871 (mCAR)), and 18 for f-RD (n=1183 (hRO), n=1105 (mCAR)). The cone-arrestin antibody failed to label cone cell bodies in the RD retinas in a reproducible manner. Therefore, subtype-specific quantifications were performed in wild-type animals. Cones are only present in the top row of the ONL. In total, 27 horizontal sections for cones (n=343 cells (hRHO), n=446 (hRO), n=463 (mCAR)) and 81 sections for rods (n=7060 cells (hRHO), n=7528 (hRO), n=7533 (mCAR)) were analyzed. Total photoreceptor cell number in a horizontal confocal optical section was obtained by counting DAPI-labeled nuclei. We determined total photoreceptor number in uninjected wild-type retinas from 24 sections (n=7169 cells) and in a NpHR transgenic mouse line from 9 sections (n=2793 cells). Estimation of persisting cone cell bodies (Fig. 3A) based on the quantification on GFP-labeled cells in P99-108 (n=5 retinas), P184-255 (n=5 retinas) s-RD, P50-77 (n=3), and P182-264 (n=3) f-RD retinas. These numbers were related to the retinal area, divided by the maximal transfection efficiency (mean + SEM) for each mouse model (s-RD 88.6%, f-RD 50.8%) and normalized to wild-type cone numbers (12,800 cells mm^{-2}, (*S17*)).

Fluorescence-activated cell sorting (FACS). Retinas from 4 mice per group (f-RD injected with mCAR-EGFP from P110 or P220 mice, and f-RD injected with mCAR-eNpHR-EYFP from P165 animals) were isolated and dissociated to single cells by papain digestion as previously described (*S18*). EGFP- or eNpHR-EYFP-positive cells were sorted using FACS (MoFlo from DakoCytomation) and used for microarray profiling.

RNA isolation and amplification, and microarray profiling. All samples were obtained in four biological replicates per genotype for microarray gene expression profiling. Following cell dissociation, cells were immediately sorted by FACS and immersed in 50 µl extraction buffer (Arcturus, USA), left to lyse at RT for 10 min and stored at -80°C. Total RNA from samples containing 500 or 300 cells was isolated using the PicoPure RNA isolation kit (Arcturus) with the following modifications. The tubes were incubated at 42°C for 10 min and vortexed at low speed. Total RNA was treated with 10 units of DNase I (Qiagen) for 15 min to remove any remaining genomic DNA and eluted in 8 µl elution buffer. The RNA quality was assessed using RNA 6000 PicoChips with the Agilent 2100 Bioanalyzer (Agilent). No traces of DNA were detected; degradation of the ribosomal RNA was absent. The rRNA represented 90–95% of total RNA and a ratio of 28S/18S equal to 1.9-2.2 was recorded, indicating that the extractions met the criteria for downstream genetic analysis. Total RNA from each sample was reverse-transcribed using 4 µM T7-(dT)24/T7-(dN)6 primer mix (Affymetrix) and 150 units Superscript II reverse transcriptase (Invitrogen) in a volume of 10 µl. Synthesis of second-strand cDNA was performed by adding 4 mM dNTPs, 6 units DNA polymerase I, and 0.4 units RNase H in a 20 µl reaction volume. cRNA was produced by *in vitro* transcription (IVT) with a T7 RNA polymerase at 37°C for 14 h using the MEGAscript T7 kit (Ambion) as per manufacturer's instructions. For the second cycle, the first-strand cDNA was synthesized using 0.2 µg random primers from 9 µl purified cRNA. The second-strand cDNA was produced using 10 µM T7-(dN)6 primer and 40 units DNA polymerase at 16°C for 2 h, after which 10 units of T4 DNA polymerase (Invitrogen) were added and incubation continued for another 10 min. The cDNA was *in vitro*-transcribed with a T7 RNA polymerase at 37°C for 16 h. The single-strand cDNA was synthesized using 10 µg purified cRNA in the presence of 4 µg random primers, 0.2 M DTT, 12 mM dNTP + dUTP, and 750 units Superscript II (Roche

Diagnostics) in a total volume of 20 µl. The cRNA was hydrolyzed with 2 units RNase H at 37°C for 40 min. The sense cDNA was purified and eluted in 28 µl elution buffer. Amplified products were purified using the GeneChip cDNA Sample Cleanup Module (Affymetrix) applying a 6,000 *g* centrifugation speed during the first two steps. To improve the recovery from the columns, water or elution buffer were spun into the matrix at 50 *g* and then left to stand for 4 min prior to 16,000 *g* centrifugation. The quantity and purity of the cRNA and cDNA produced during the first and second rounds were evaluated using the NanoDrop ND-1000 spectrophotometer (Nanodrop Technologies). The cDNA was then fragmented using UDG (uracil DNA glycosylase) and APE 1 (apurinic/apyrimidic endonuclease 1), and biotin-labeled with TdT (terminal deoxynucleotidyl transferase) using the GeneChip WT Terminal labeling kit (Affymetrix). Hybridization was performed using 5 µg biotinylated target, which was incubated with the GeneChip Gene 1.0 ST array (Affymetrix) at 45°C for 16 h. Following hybridization, nonspecifically bound nucleotides were removed by washing, and detection of specifically bound target was performed using the GeneChip Hybridization, Wash and Stain kit, and the GeneChip Fluidics Station 450 (Affymetrix). The arrays were scanned using the GeneChip Scanner 3000 7G (Affymetrix), and CEL files acquired using the GeneChip Command Console Software (Affymetrix). Quality control and gene expression value estimates were obtained after Robust Multichip Analysis (RMA) and quantile normalization performed in R (version 2.10). To identify transcripts that are differentially expressed between the controls and the mutant mice, we defined a criterion of a 2-fold or greater difference, plus a P-value of < 0.01.

Human ocular tissue. Human ocular tissue from individuals without known eye diseases was obtained from the Cornea Bank of Amsterdam and was handled in accordance with the guidelines of the Declaration of Helsinki. Eyes were collected from five donors (ranging in age from 58 to 65 years) after death through natural causes. After removal of the cornea,

eyes were put into storage within 6 to 12 h in cold phosphate-buffered saline solution (PBS) and shipped to Basel where the experiments took place. Retinas were always put into culture less than 36 h *post-mortem*.

Human retinal explant culture and vector administration. Immediately after the arrival of the eyes, the anterior parts were removed and the vitreous humor with attached neural retina was transferred to a CO_2-independent medium (Invitrogen). The retina was separated from the vitreous humor and from the retinal pigment epithelium, and cut into ~1 cm² pieces. With the photoreceptor face up, these retinal pieces were placed on the polycarbonate membrane of a Transwell 0.4 μm cell culture insert (Corning) with one drop of CO_2-independent medium, and flattened with a polished Pasteur pipette. Next, the CO_2-independent medium was removed, and 2 ml neurobasal-A medium with 2mM L-glutamine plus B27 supplement (NBA+; Invitrogen) were added to each well. 10-50 μl AAV (3×10^{12} to 5×10^{12} GC ml^{-1}, see Supplementary Table S3) or 10 μl lentivirus (2×10^{9} VG ml^{-1}) were added on top of the retinal explants. Virus-infected retinas were incubated for up to 18 days for AAVs, and 24-72 h for lentivirus. The culture medium was renewed by a daily addition of fresh NBA+ medium to each well. Human retinas were already light insensitive at the time of isolation.

Light stimulation of isolated retinas. Light generated by a 120W epifluorescent mercury lamp-based illuminator (X-Cite 120PC, EXFO Photonics Solutions) was filtered with a band-pass filter (600-660 nm, Chroma Technology) and projected onto the retina. The light path was interrupted with a computer-controlled shutter (SC10, Thorlabs). Light intensity was modulated by neutral density filters over a range of 5 log units (ND 0-ND 40). For patterned light stimuli, the retina was stimulated using a digital light projector (V-332, PLUS Vision) filtered with the same band-pass filter used for the epifluorescent light path.

A monochromatic light source (15nm bandwidth, TILL Photonics Polychrome V, Agilent Technologies) was used to provide a color-ramp, light flashes, or periodic light pulses at defined wavelengths. The color-ramp started at 400 nm and continuously increased to 650 nm within 5 s. Light intensities from all three light sources were measured using a fluorescent spectrometer (USB 4000, Ocean Optics) calibrated with a radiometric reference source (LS1-Cal, Ocean Optics). The stimulus was generated via custom-made software written by D.B. (Matlab, Mathworks and Labview, National Instruments).

Two-photon targeted patch clamp recordings. AAV-transduced retinas from s-RD and f-RD mice were isolated in Ringer's medium (110mM NaCl, 2.5mM KCl, 1mM $CaCl_2$, 1.6mM $MgCl_2$, 10mM D-glucose, and 22mM $NaHCO_3$, bubbled with 5% CO_2/95% O_2). For photoreceptor patch clamp recordings, retinal slices (200 μm) were cut with a razor blade tissue chopper (Stoelting) and placed in the recording chamber of the microscope. The tissue was superfused in Ringer's medium at 36°C for the duration of the experiment. AAV-transduced fluorescent photoreceptors were targeted with a patch electrode using a custom-made 2-photon microscope. A CCD camera was used to visualize the retina (illuminated with infrared light, 725-775 nm) during two-photon scanning. Whole-cell recordings were made using an Axon Multiclamp 700B amplifier. Patch electrodes were made from borosilicate glass (BF100-50-10, Sutter Instruments) pulled to 8-10 MΩ, and filled with 115mM K Gluconate, 10mM KCl, 1mM $MgCl_2$, 0.5mM $CaCl_2$, 1.5mM EGTA, 10mM HEPES, and 4mM ATP-Na_2 (pH 7.2). In f-RD retinas the photoreceptor recordings were only performed on cones, since rods died before our recordings. In s-RD retinas we used two criteria to identify cones before the recordings. First, since cone cell bodies occupy only the most distal row of the outer nuclear layer we recorded from cell bodies in this row. Second, since cone cell bodies are larger than rod cell bodies we only targeted the largest cell bodies. In a few cases we verified that we recorded from cones by filling the

recorded cell with Lucifer yellow, which showed the characteristic axon terminals of cones. We cannot rule out completely the possibility that some of the recorded cells in s-RD retinas were rods.

For ganglion cell recordings, the retina was mounted ganglion-cell-side up on a piece of filter paper (MF-membrane, Millipore) with a 2 mm^2 opening in the middle. Ganglion cell spike recordings were performed with a loose cell-attached patch, using the same electrodes pulled to 6-8 MΩ, and filled with Ringer's medium. Excitatory currents were isolated by voltage clamping ganglion cells at the reversal potential of Cl^- (-60 mV) (*S16*). For these recordings, electrodes were filled with 112.5mM $CsMeSO_4$, 1mM Mg SO_4, 7.8×10^{-3} mM $CaCl_2$, 0.5mM BAPTA, 10mM HEPES, 4mM ATP-Na_2, 0.5mM GTP-Na_3, 5mM lidocaine N-ethyl bromide (QX314-Br), and 7.5mM neurobiotin chloride (pH 7.2). To record spikes and currents, or to record spikes and obtain the morphology of ganglion cells, we first performed cell-attached recordings. Next, we broke into the recorded cell using another electrode filled with intracellular solution containing neurobiotin in whole-cell mode and either recorded currents or simply filled cells with neurobiotin for subsequent anatomical analysis. For human photoreceptor patch clamp recordings, we used human retinal explants, which were incubated with the lentiviral vectors for 1-2 days. The human retinas were cut into slices (200 μm) with a razor blade tissue chopper using the method described above. Brightly labeled photoreceptors from the parafoveal region were targeted with a patch electrode (8-10 MΩ) filled with 115mM K gluconate, 10mM KCl, 1mM $MgCl_2$, 0.5mM $CaCl_2$, 1.5mM EGTA, 10mM HEPES, and 4mM ATP-Na_2 (pH 7.2). Patch-clamp recordings were also made from non-transduced human photoreceptors immediately after the isolation of the retina. The human tissue was superfused in Ringer's medium at 36°C for the duration of the patch-clamp experiment. All chemicals were obtained from Sigma, with the exception of ATP (Labforce) and neurobiotin (Vector Laboratories). Data were

analyzed offline using Matlab (Mathworks). For statistics, we averaged over ON and OFF responses. The direction-selectivity index shown in Fig. 4D is computed as described (*S19*).

Multi-electrode array recordings. To record the spike trains of retinal ganglion cells, the isolated mouse retina was placed on a flat MEA60 200 Pt GND array with 30 μm diameter microelectrodes spaced 200 μm apart (Ayanda Biosystems or Multi Channel Systems). The retina was continuously superfused in oxygenated Ringer's solution (110mM NaCl, 2.5mM KCl, 1.0mM $CaCl_2$, 1.6mM $MgCl_2$, 22mM $NaHCO_3$, and 10mM D-glucose (pH 7.4 with 95% O_2/5% CO_2)) at 36ºC during experiments. Recordings ranged from 1 to 5 h in duration. The signals were recorded (MEA1060-2-BC, Multi-Channel Systems) and filtered between 500 Hz (low cut-off) and 3,500 Hz (high cut-off). The spikes were extracted with a threshold of at least 4 times the standard deviation of the recorded trace (Matlab, Mathworks).

Visual-evoked potentials. Mice (ages s-RD: P70-P99, f-RD: P67-P118, wild-type: P42-P60) were anesthetized by subcutaneous injection of 8% chloral hydrate. Atropine drops (1%) and Oculotect (Novartis) were applied to the right eyes to dilate and protect the pupils. After exposing the primary visual cortex (V1), platinum-iridium recording electrodes (size 0.0035, California Fine Wire Company) were inserted. Responses were first measured at different cortical depths, and the depth with the maximum response was chosen for further recordings. 500 ms light stimulus was delivered to the contralateral eye every 3 seconds, 30 times, using an optical cable attached to a band pass filtered (D595/40, Chroma Technology) light source (EXFO XI120PC-XL, 120W, Photonic Solutions). The distance of the tip of the optical cable from the eye was 1 cm. The intensity of light was 10^{16} photons cm^{-2} s^{-1} at the eye surface. Each neural response was band-pass filtered at 0.1-500 Hz.

Dark-light box. Mice (ages s-RD: P44-P143, f-RD: P50-P120, wild-type: P52-P64, female) were kept under a 12-hour light-dark cycle and tested between 9 a.m. and 12 p.m. Movement of mice in the dark-light box was recorded with a wireless infrared camera (SA-6255, Stilus SA) equipped with a longpass-filter (FGL665, Thorlabs) and digitized at 25 frames s^{-1} (AV400MKII, TerraTec Electronic GmbH). The interior dimensions of the dark-light box were 32(width)×40(length)×22(height) cm. We inserted a non-transparent wall with a 7×3 cm hole (the hole was at the bottom of the wall in the middle) in the middle of the box, creating two equal-sized compartments (32(width)×20(length)×22(height) cm). One compartment was illuminated from the top with two red LED arrays (OD-610-99-070, Opto Diode), while the other remained dark (<2 lux). Illumination in this "light compartment" could be adjusted between 2 and 2,000 lux. Mice were placed individually in the corner of the light compartment and allowed to freely explore the box. The movement of the animal was recorded for 5 min. The mouse's head was used to define the compartment it occupied. The time spent in each compartment was recorded. RD animals (eNpHR- or EGFP-expressing) spent a variable amount of time in the light compartment before the first crossing. This increased the variance of the total time spent in the light or dark compartment. We eliminated this time in our analysis by calculating the time in light compartment as (total time in light compartment - time until the first crossing) / (total recording time - time until the first crossing). This modification introduced a slight preference for the dark compartment. Results were, however, still statistically significant without this correction.

Optomotor response. The experiment was carried out as previously described (*S4, S20*) with small modifications. Briefly, each mouse (ages s-RD: P113-P153, f-RD: P69-P120, wild-type: P52-P64, female, kept in a 12-hour light-dark cycle, tested between 9 a.m. and 3 p.m.) was placed on an elevated (20cm high) platform (9cm diameter) which was

positioned in the middle of an optokinetic drum (30cm diameter, 40 cm height). The drum was made of transparent plastic and decorated with black vertical stripes of different widths corresponding to different cycles per degree (cpd) spatial frequencies (0.03, 0.07, 0.13, 0.26, 0.52 cpd) and rotated with a predetermined number (1, 2, 3, 4, 7) of revolutions per minute (rpm). The platform did not rotate. The drum was illuminated from outside with 6 red LED arrays (OD-610-99-070, Opto Diode) that generated 2,000 lux at the position of the animal's head. The contrast was 1:23 using the 0.26 cpd drum. During the test, the drum turned clockwise and then anti-clockwise for 2 min in each direction. This procedure was repeated at every spatial frequency at 2 rpm and every rotational speed at 0.13 cpd. Mice were recorded using the same video recorder and capture board as described above in the context of the dark-light box. We analyzed all head movements which lasted more than 400 ms. If the speed of the head (estimated as different angular positions within 400 ms) was within ±15% of the angular speed of the drum for more than 320 ms then the mouse was given a score of +1, if not it received -1. These points were added together to form a total score for the 2+2 min recording period. All RD analysis was done in an automated fashion by a program written in Matlab (Mathworks). Wild-type optomotor scores from female animals were obtained manually as previous described (*S20*). Note that in our automatic scoring procedure we added penalty points to head movements in the direction opposite to the motion of the drum, while in the manual scoring we followed the procedure used by (*S20*), which simply counts the slow head movements in the direction of motion of the drum. Therefore the absolute values of the scores are not comparable.

Optical coherence tomography (OCT). OCT and functional tests (see below) were performed at the Center for Clinical Investigation (CIC) of the Centre Hospitalier National d'Ophtalmologie des Quinze-Vingts in Paris. OCT imaging was carried out using spectral domain OCT (Spectralis® OCT, Heidelberg Engineering, Dossenheim, Germany).

Goldmann perimetry. Photopic visual field measurements were performed with a Goldmann perimeter (Haag-Streit AG, Bern, Switzerland). The kinetic perimetry was performed by moving the tests IV1, V1, and V4 from non-seeing to seeing areas. The visual field areas were then determined after plotting the fields with a desktop planimeter.

Statistical analysis. If the Lilliefors test did not reject the hypothesis that the sample had a normal distribution at the 5% significance level and $n>7$, then the statistical significance was determined using a one-tailed heteroscedastic Student's t-test. Otherwise the Wilcoxon rank-sum test was used. We used the Kruskal-Wallis non-parametric 1-way ANOVA test to compare groups. The significance levels are indicated by * for $p < 0.05$, ** for $p < 0.01$, and *** for $p < 0.001$. The error bars and ± values represent s.e.m.

Supplementary figures

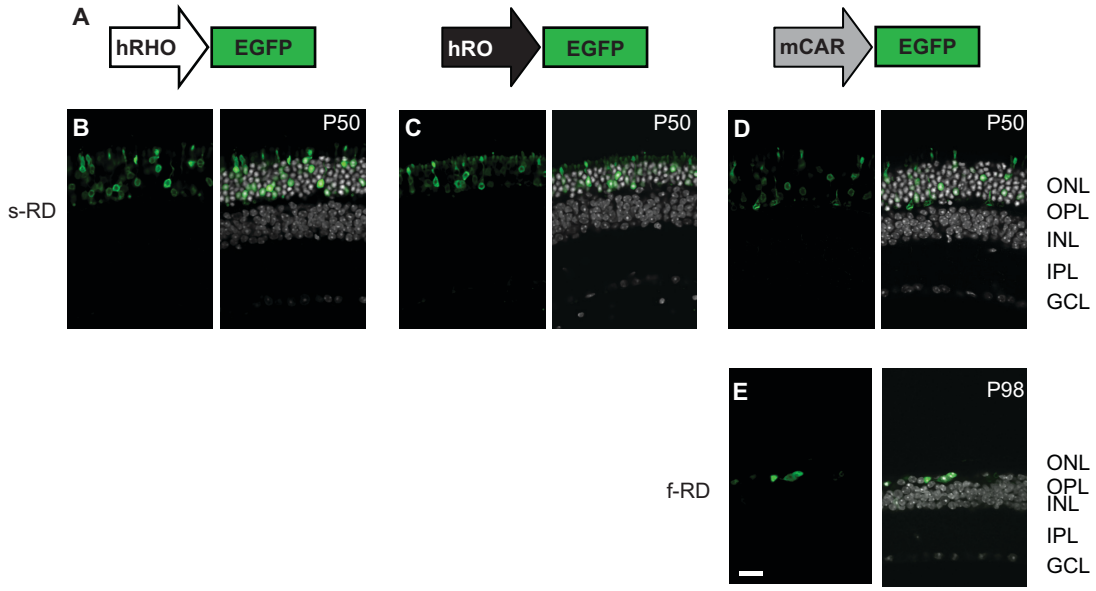

Supplementary Figure 1. (**A**) EGFP-expressing control AAV vectors. (**B-E**) Cross-sections of hRHO-EGFP- (**B**), hRO-EGFP- (**C**), mCAR-EGFP- (**D**) transduced s-RD and mCAR-EGFP- (**E**) transduced f-RD retinas. Scale bar 20 μm.

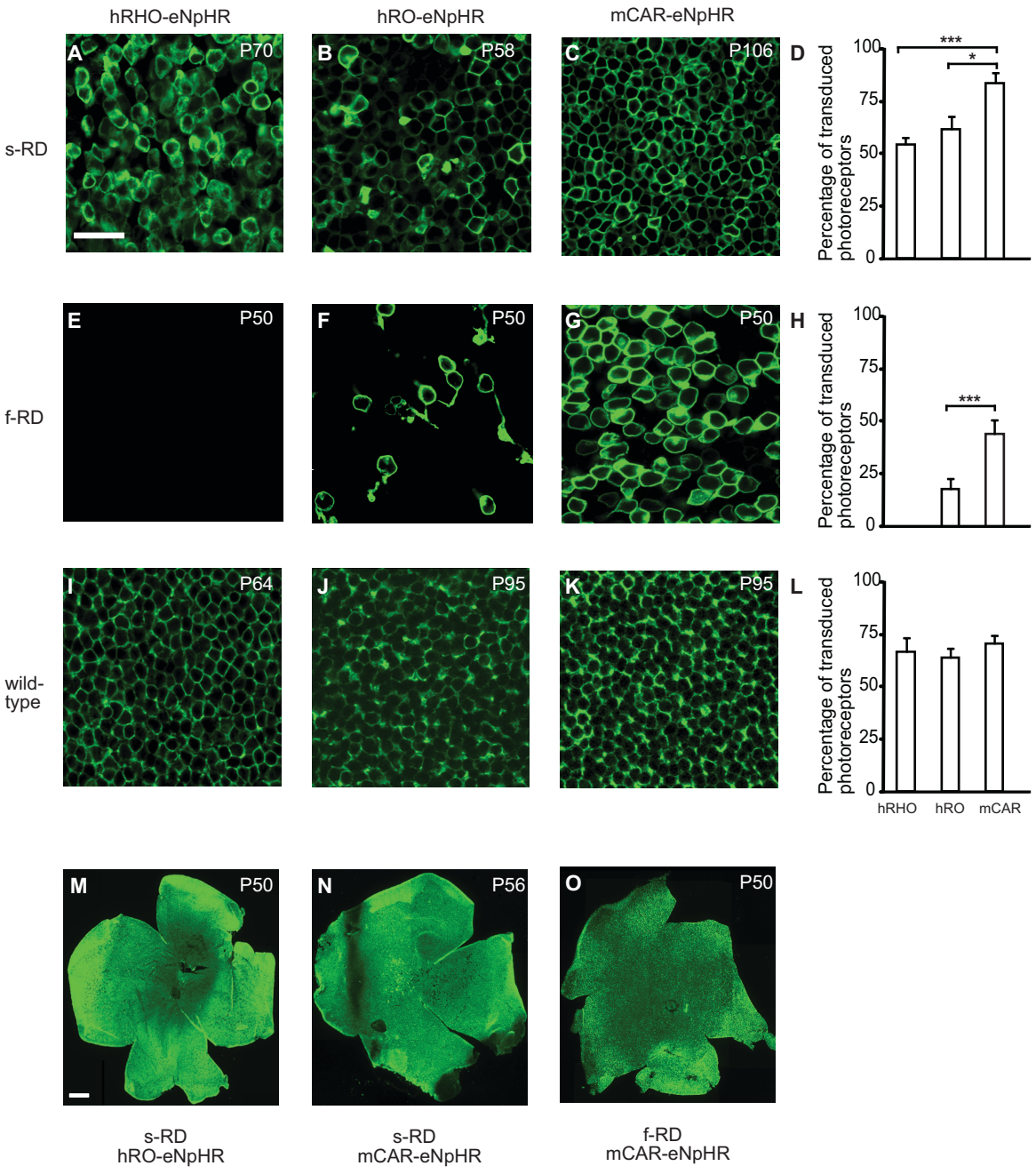

Supplementary Figure 2. Efficiency of eNpHR expression from different promoters. Confocal top views of eNpHR-EYFP expressing, GFP-immunostained photoreceptors in s-RD (**A**-**C**), f-RD (**E**-**G**) and wild-type (**I**-**K**) retinas, promoters are indicated above. Scale bar 20 µm. (**D**, **H**, **L**) Percentage of transduced photoreceptors with different promoter constructs. (**M**-**O**) Confocal tile scans of GFP-immunostained s-RD (**M**, **N**) and f-RD (**O**) retinas. Scale bar 250 µm.

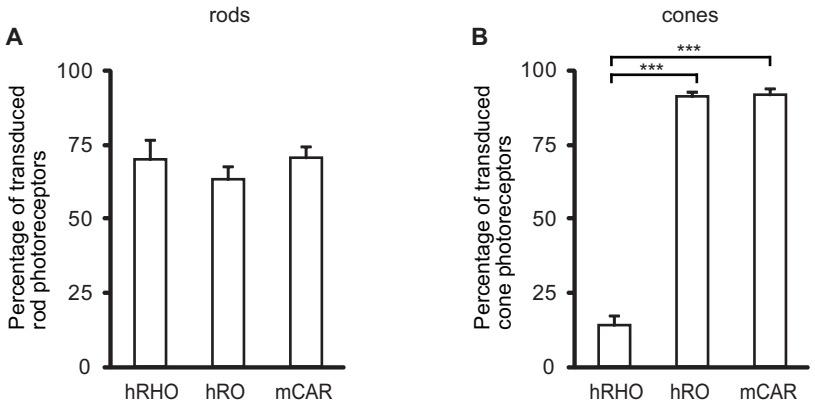

Supplementary Figure 3. The efficiency of cone photoreceptor targeting. (**A**, **B**) Percentage of transduced rods (**A**) and cones (**B**) by different promoter constructs quantified in wild-type retinas.

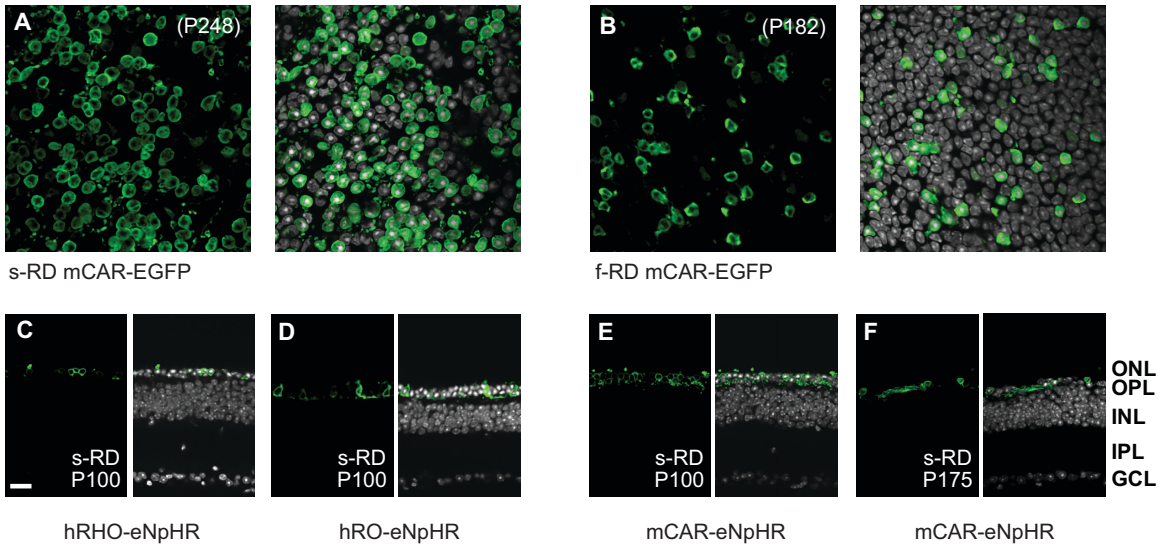

Supplementary Figure 4. Persisting eNpHR-EYFP or EGFP expression in RD retinas (P100-P248). (**A**, **B**) Left, confocal top view of GFP-immunostained s-RD (**A**) and f-RD (**B**) photoreceptors transduced by mCAR-EGFP. Right, co-stained with DAPI. (**C**-**F**) Cross-sections of GFP-immunostained s-RD retinas transduced by hRHO- (**C**), hRO- (**D**), and mCAR- (**E**, **F**) eNpHR-EYFP AAVs at P100 (**C**-**E**) and P175 (**F**, only mCAR-eNpHR is shown). Scale bar 20 μm.

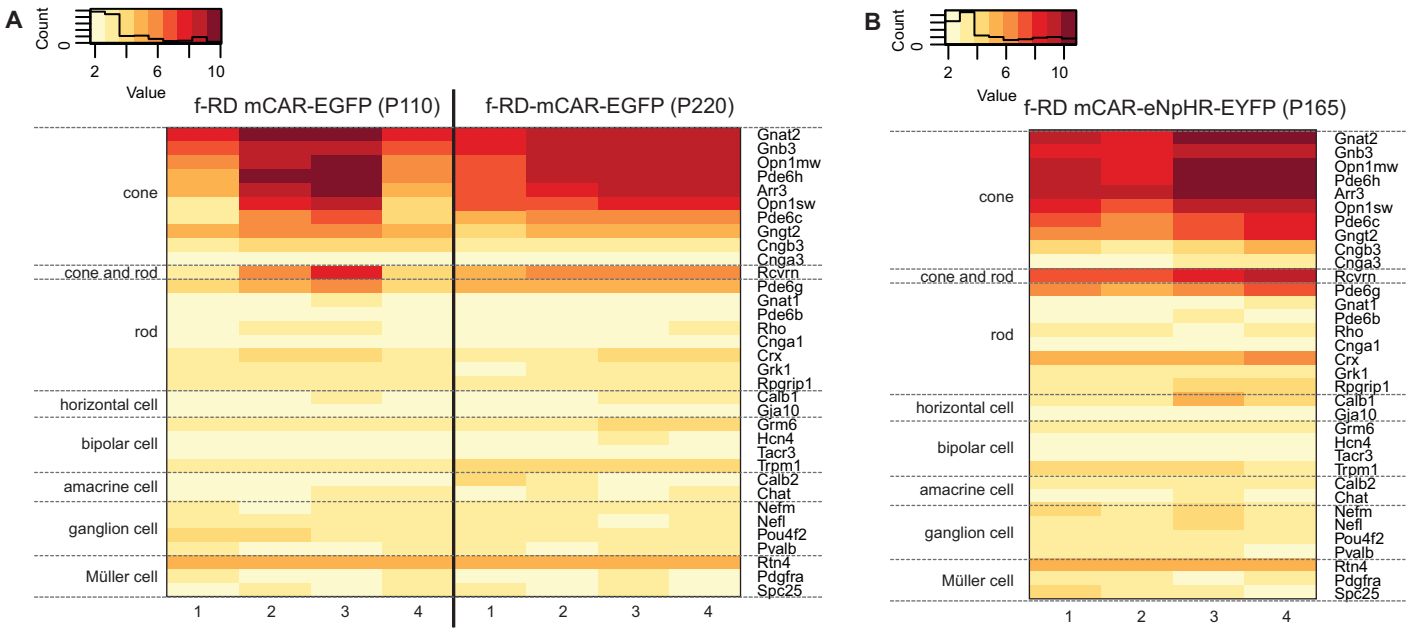

Supplementary Figure 5. Analysis of the transcriptome of eNpHR-EYFP and EGFP expressing cells in f-RD retinas. (**A**) Microarray analysis of EGFP-expressing and FACS-sorted f-RD photoreceptors (from P110 and P220 mice, in quadruples), heat map shows known cone markers (*S21*) and additional retinal cell-type markers. (**B**) Microarray analysis of eNpHR-EYFP-expressing FACS-sorted f-RD photoreceptors (from P165 mice, in quadruples).

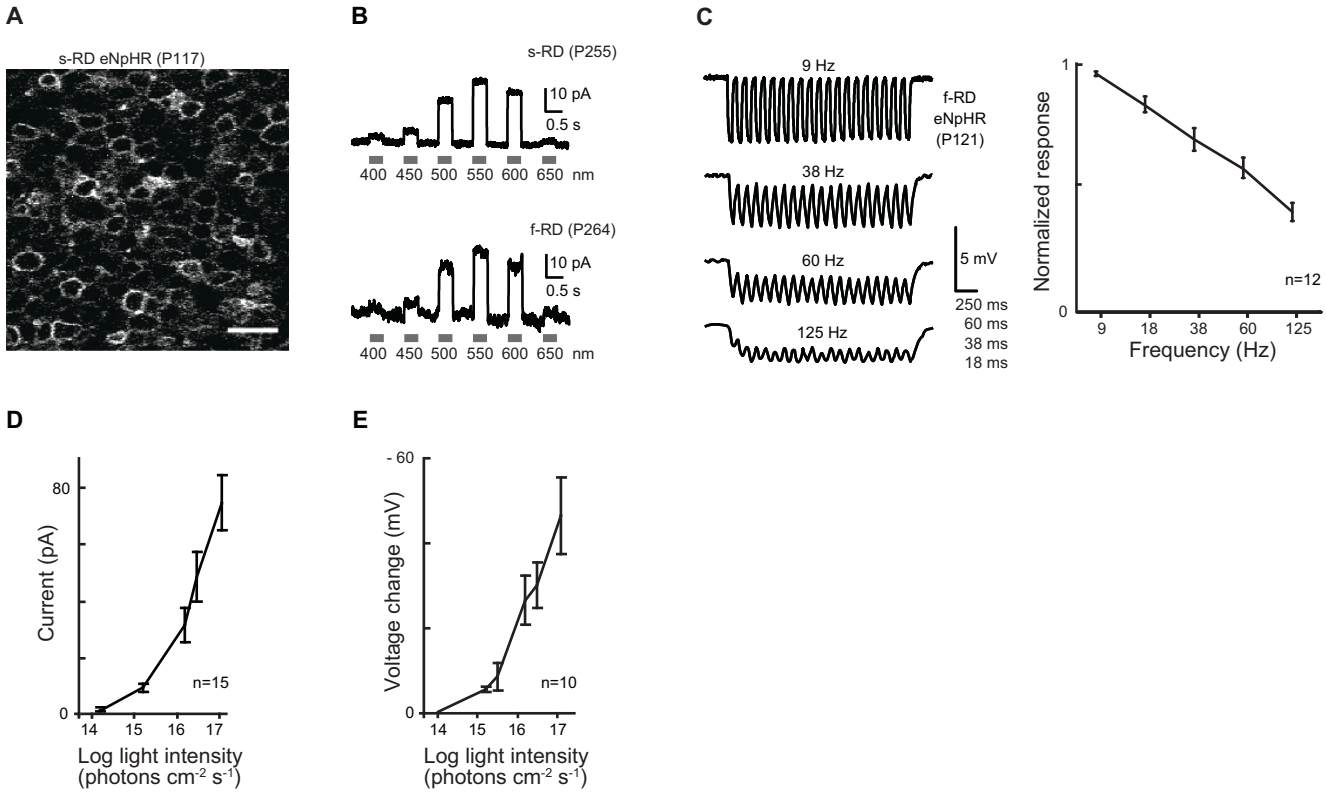

Supplementary Figure 6. Functional properties of the light responses of the eNpHR-expressing RD photoreceptors. (**A**) Two-photon laser scanning live image of photoreceptor cells expressing eNpHR-EYFP driven by the hRO promoter in an AAV-injected s-RD retina. Scale bar 10 µm. (**B**) Action spectrum of eNpHR-expressing P255 s-RD (top) and P264 f-RD (bottom) photoreceptors stimulated by full-field light flashes; gray bars indicate the timing of the stimulus. (**C**) Left, eNpHR-mediated modulation of photoreceptor membrane voltage from 9 to 125 Hz; right, normalized voltage response as a function of stimulus frequency (580 nm light). (**D**, **E**) Light-evoked changes of current (**D**) and membrane voltage (**E**) as a function of light intensity. "n" refers to the number of different cells we measured from.

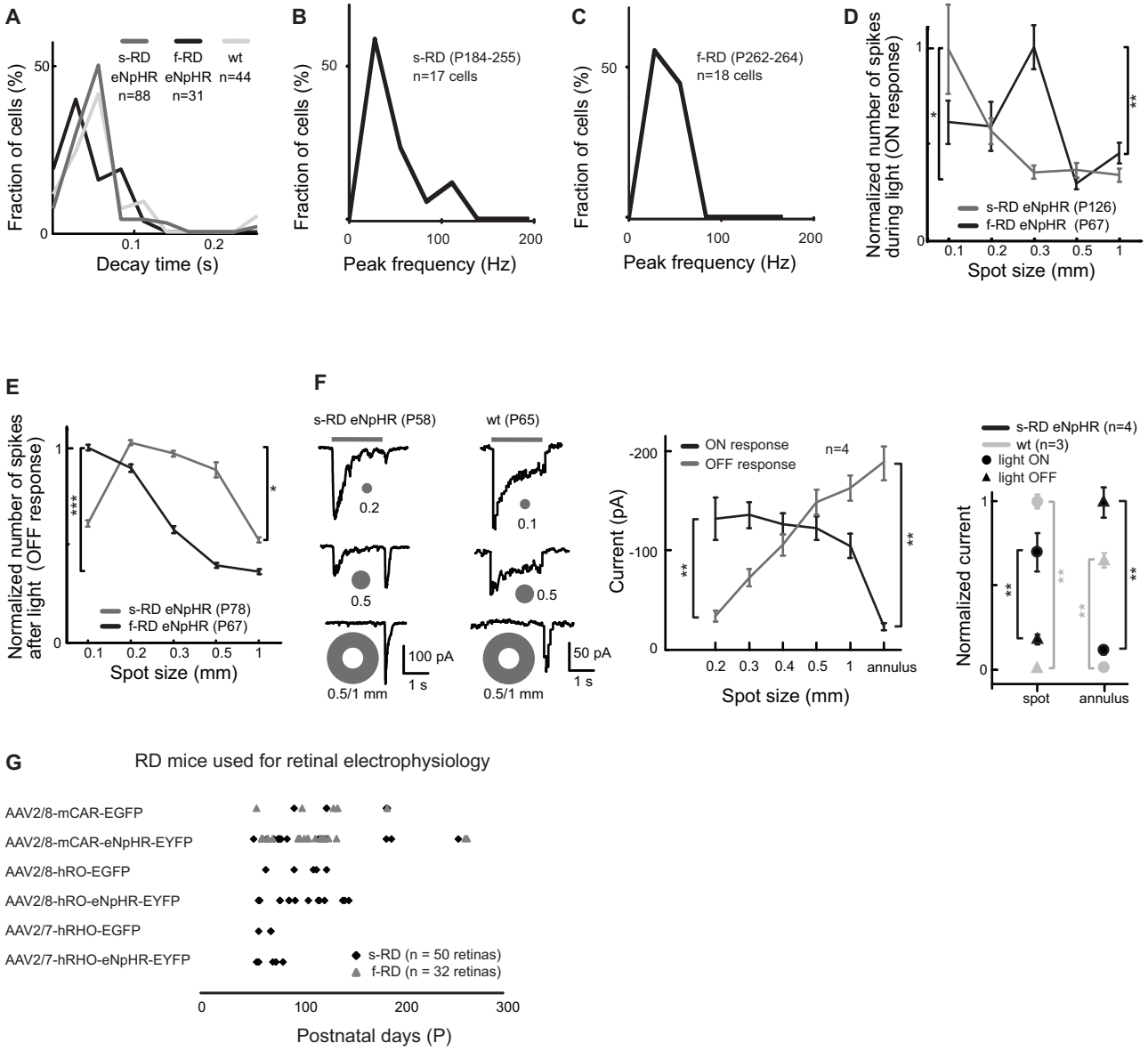

Supplementary Figure 7. The properties of light responses of ganglion cells in eNpHR-expressing RD retinas. (**A**) Both transient and more sustained ganglion cell responses can be recorded in eNpHR-transduced RD retinas. Distribution of the estimated decay time of the spike frequency response to full-field flashes in s-RD, f-RD, and wild-type (wt) retinas (difference between groups is not significant, p=0.17). (**B**, **C**) Spiking frequency distribution in ganglion cells of eNpHR-transduced P184-255 s-RD (**B**) and P262-264 f-RD (**C**) retinas. Full-field light stimuli. (**D**, **E**) The effect of lateral inhibition. Examples from four ganglion cells. Number of spikes (normalized to the mean of the peak response) as a function of stimulus diameter in ON-type (**D**) and OFF-type (**E**) ganglion cells. (**F**) Left, an 'ON centre OFF surround' response in ganglion cells of an s-RD and a wild-type retina. Excitatory currents evoked by stimulation with increasing spots and an annulus. Gray bars indicate the timing of the light stimulus. Note that the receptive field center stimulation with a spot evokes an ON response and the receptive field surround stimulation evokes an OFF response. Middle, magnitude of excitatory currents for the ON-centre and OFF surround responses as a function of stimulus size in s-RD ganglion cells. Right, comparison to wild-type responses. "n" refers to the number of different cells we measured from. (**G**) Age of AAV-injected RD mice used for testing light responses. Each row represents recordings with a particular AAV type, indicated on the left. The timeline at the bottom labels the age of RD mice. Each rectangle (s-RD) or triangle (f-RD) refers to recordings on a particular postnatal day.

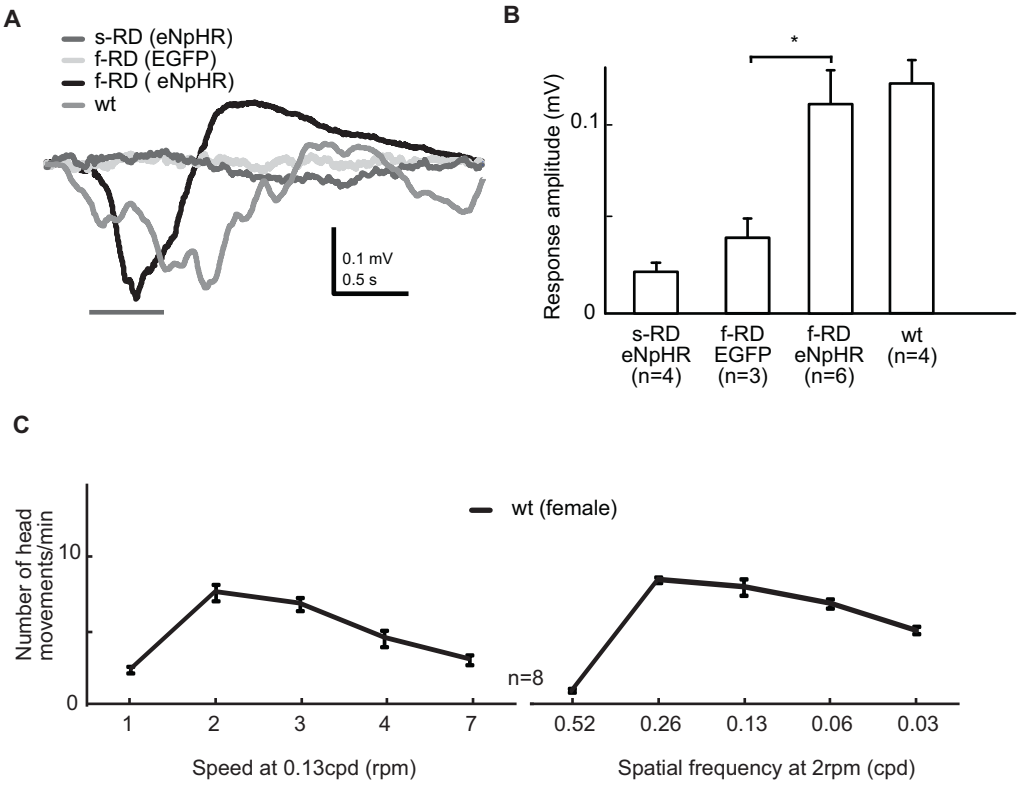

Supplementary Figure 8. Visually evoked potentials (VEPs) in eNpHR-expressing RD and wild-type mice (wt). (**A**) Examples of VEPs recorded in the visual cortex. (**B**) VEP response amplitudes. The intensity of light was 10^{16} photons cm^{-2} s^{-1} at the eye surface (**C**) Optomotor response score of female wild-type mice (*S20*) at different rotational speeds and spatial frequencies. "n" refers to the number of different animals we measured from.

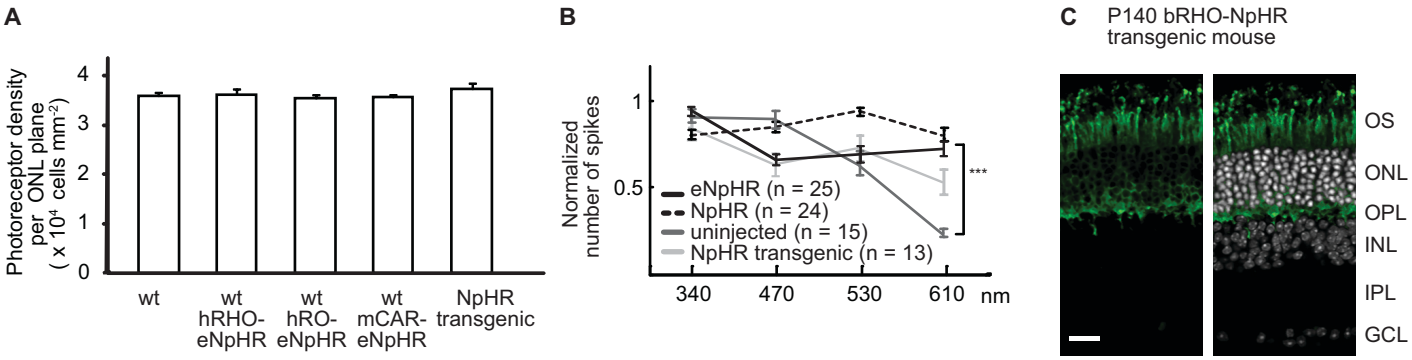

Supplementary Figure 9. eNpHR and NpHR expression is not cytotoxic to wild-type photoreceptors. (**A**) Photoreceptor density measured in confocal horizontal planes (see Materials and methods) of uninjected wild-type (wt), wild-type injected with three different eNpHR-EYFP-expressing AAVs, and bRHO-NpHR-EYFP transgenic mice. (**B**) Action spectra of AAV-transduced wild-type retinas with eNpHR (black, merged hRO and mCAR), NpHR (dashed black, hRHO), uninjected wild-type retinas (dark gray), and bRHO-NpHR-EYFP transgenic retinas (light gray) by multi-electrode array recordings. "n" refers to the number of different cells we measured from. (**C**) Cross-section of a bRHO-NpHR-EYFP transgenic mouse retina (P140). Left, EYFP signal; right, merged with DAPI. Scale bar 20 μm.

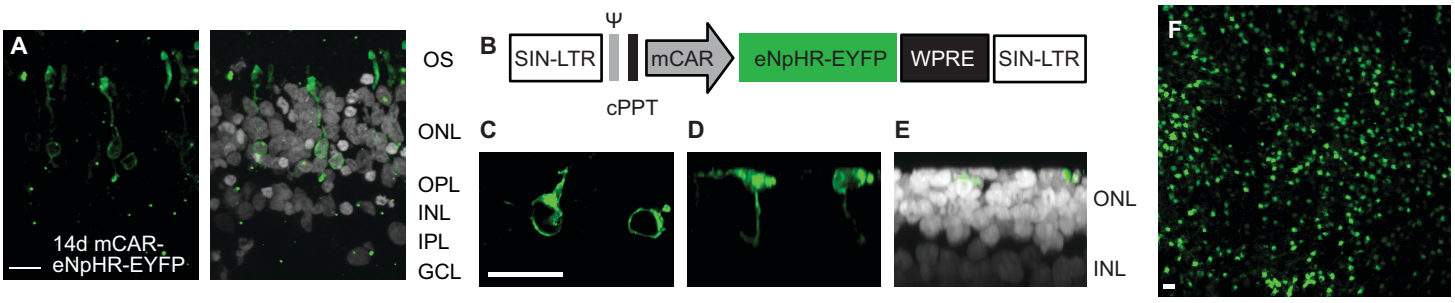

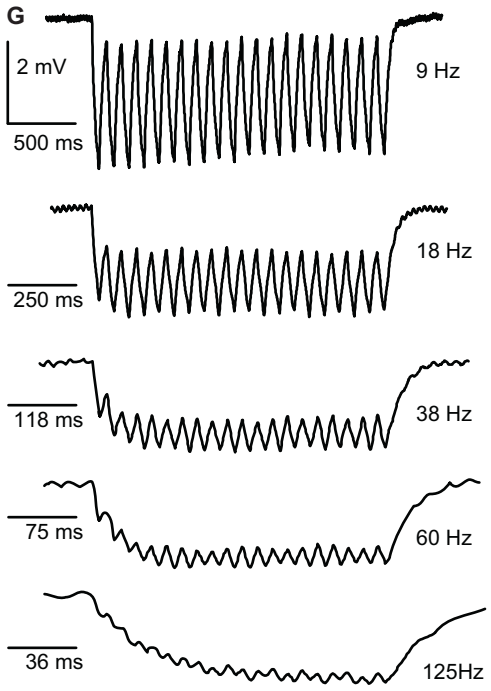

Supplementary Figure 10. Viral targeting of photoreceptors in *ex vivo post-mortem* human retinal cultures. (**A**) Left, confocal cross-section of GFP-immunostained AAV-transduced eNpHR-EYFP-expressing human photoreceptors. Right, merged with DAPI staining (white). (**B**) Lentiviral eNpHR-EYFP expression construct: SIN-LTR, self-inactivating long tandem repeat; ψ, extended packaging signal; cPPT, central polypurine tract; WPRE, woodchuck hepatitis virus post-transcriptional regulatory element. (**C**-**E**) Confocal image of GFP-immunostained (green) photoreceptors. Top view (**C**), side view (**D**), and side view together with DAPI staining (white, **E**). (**F**) Confocal image (top view) of a lentivirus-transduced area of a human retina after 7 days in culture and 2 days after lentiviral administration. Scale bars 20 µm. (**G**) eNpHR-mediated modulation of human photoreceptor membrane voltage with light pulses from 9 to 125 Hz.

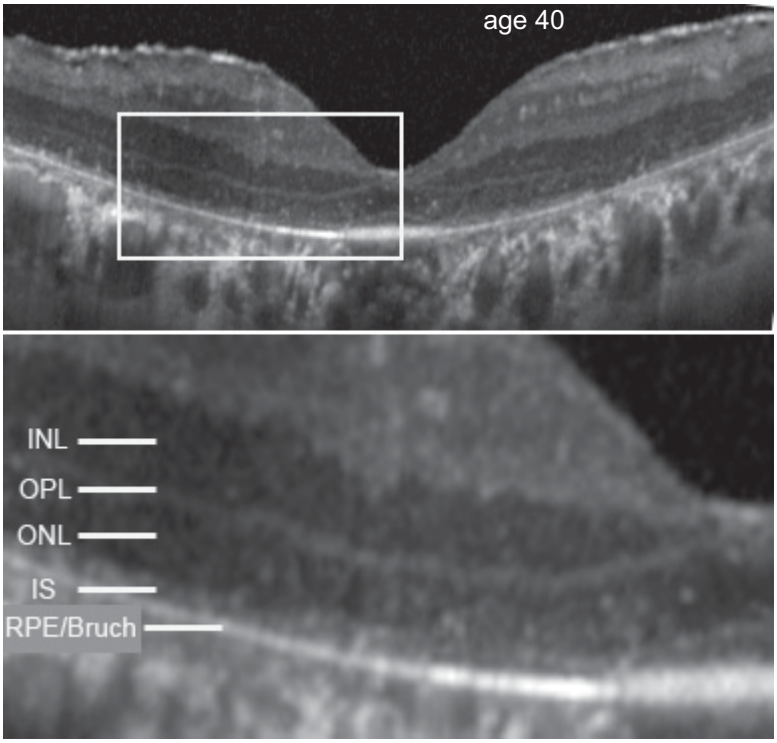

Supplementary Figure 11. Enlarged view of the OCT image of the patient shown in Fig. 6F. Left eye of a 40 year-old man with sporadic RP. Loss of vision since the age of 15. Visual acuity, hand motion. Flat ERG. No detectable visual field. While the ONL and inner segments (IS) are clearly delineated, there are no detectable outer segments. The retinal pigment epithelium (RPE) and the Bruch membrane are indicated.

Supplemetary Table S1: Range of mice used for experiments

Experiment	s-RD	f-RD	wild-type
Imaging	P50-P255	P50-264	P64-93
Retinal electrophysiology	P53-P255	P56-264	P30-180
Cortical recordings	P70-99	P67-118	P42-60
Dark/light box test	P44-143	P50-120	P52-64
Optomotor test	P113-153	P69-120	P52-64

Supplemetary Table S2: Sources of plasmids

Construct name	Source
pAAV2.1-Rho-eGFP	Alberto Auricchio
Lenti-CaMKIIa-eNpHR-EYFP-WPRE	Karl Deisseroth
pcDNA3.1/NpHR-EYFP	Karl Deisseroth
pRed2.1lacZ	Jeremy Nathans
pRho-dsRed	Constance Cepko
pRRLsincPPT-hPGK	Didier Trono

Supplemetary Table S3: AAV constructs

AAV sample	Serotype	Promoter	Transgene	Titer [GC/mL]
AAV2-hRHO-EGFP	7	hRHO	EGFP	3.81×10^{12}
AAV2-hRHO-eNpHR-EYFP	7	hRHO	eNpHR-EYFP	3.28×10^{12}
AAV2-hRO-EGFP	8	hRO	EGFP	4.51×10^{13}
AAV2-hRO-eNpHR-EYFP	8	hRO	eNpHR-EYFP	3.08×10^{12}
AAV2-mCAR-EGFP	8	mCAR	EGFP	5.36×10^{13}
AAV2-mCAR-eNpHR-EYFP	8	mCAR	eNpHR-EYFP	5.33×10^{12}

Supplemetary Table S4: Antibodies

Primary antibody	Species	Dilution	Company	Stock #
anti choline acetyltransferase (ChAT)	goat	1:200	Chemicon	AB144P-200UL
anti cone arrestin	rabbit	1:200	MA Dyer, C Craft	
anti green fluorescent protein (GFP)	rabbit	1:200	Invitrogen	A 11122
anti green fluorescent protein (GFP)	sheep	1:200	Biogenesis	4745-1051
Secondary antibody				
anti goat IgG (H+L)-Alexa Fluor 633	donkey	1:200	Invitrogen	A21082
anti rabbit IgG (H+L)-Alexa Fluor 488	donkey	1:200	Invitrogen	A21206
anti sheep IgG (H+L)-Alexa Fluor 488	donkey	1:200	Invitrogen	A11015
anti rabbit IgG (H+L)-Cy3	donkey	1:300	Jackson Labs	711-165-152

Supporting references and notes

S1. B. Povazay *et al.*, *Opt Express* **17**, 4134 (Mar 2, 2009).
S2. A. H. Milam, Z. Y. Li, R. N. Fariss, *Prog Retin Eye Res* **17**, 175 (Apr, 1998).
S3. A. Bi *et al.*, *Neuron* **50**, 23 (Apr 6, 2006).
S4. P. S. Lagali *et al.*, *Nat Neurosci* **11**, 667 (Jun, 2008).
S5. S. G. Jacobson *et al.*, *Invest Ophthalmol Vis Sci* **51**, 1079 (Feb).
S6. P. Degenaar *et al.*, *J Neural Eng* **6**, 035007 (Jun, 2009).
S7. N. Grossman *et al.*, *J Neural Eng* **7**, 16004 (Feb).
S8. B. Y. Chow *et al.*, *Nature* **463**, 98 (Jan 7).
S9. U. B. Kaupp, R. Seifert, *Physiol Rev* **82**, 769 (Jul, 2002).
S10. V. Gradinaru, K. R. Thompson, K. Deisseroth, *Brain Cell Biol* **36**, 129 (Aug, 2008).
S11. Y. Wang *et al.*, *Neuron* **9**, 429 (Sep, 1992).
S12. X. Zhu *et al.*, *FEBS Lett* **524**, 116 (Jul 31, 2002).
S13. T. Matsuda, C. L. Cepko, *Proc Natl Acad Sci U S A* **101**, 16 (Jan 6, 2004).
S14. F. Zhang *et al.*, *Nature* **446**, 633 (Apr 5, 2007).
S15. R. Zufferey, D. Nagy, R. J. Mandel, L. Naldini, D. Trono, *Nat Biotechnol* **15**, 871 (Sep, 1997).
S16. T. A. Munch *et al.*, *Nat Neurosci*, (Sep 6, 2009).
S17. C. J. Jeon, E. Strettoi, R. H. Masland, *J Neurosci* **18**, 8936 (Nov 1, 1998).
S18. J. M. Trimarchi *et al.*, *J Comp Neurol* **502**, 1047 (Jun 20, 2007).
S19. W. R. Taylor, D. I. Vaney, *J Neurosci* **22**, 7712 (Sep 1, 2002).
S20. J. Abdeljalil *et al.*, *Vision Res* **45**, 1439 (May, 2005).
S21. J. C. Corbo, C. A. Myers, K. A. Lawrence, A. P. Jadhav, C. L. Cepko, *Proc Natl Acad Sci U S A* **104**, 12069 (Jul 17, 2007).

V.B. developed the plasmids and viral vectors, performed in vivo AAV injections in mice, in vitro lentiviral infections of human retinas, immunohistochemistry, confocal microscopy, image processing, transfection quantifications, multielectrode array recordings, and behavioral assays, designed experiments, and wrote the paper. J.D. performed the two-photon targeted patch-clamp experiments of cones and ganglion cells in mice and cones in human retinas, helped with behavioral assays, designed experiments, and wrote the paper. D.B., who sadly passed away during the preparation of the paper, performed multielectrode array recordings, cortical recordings, and behavioral experiments, developed recording and analysis software, designed experiments, and wrote the paper. M.F., V.F., J.A.S., and S.P. developed the conditions for human retinal cultures, isolated and cultured human retinas, and performed immunohistochemistry. T.J.V. and S.S. performed ganglion cell patch clamp experiments. E.C. performed gene chip experiments. S.S. analyzed gene chip data. A.C.G. and D.T. made the lentiviral particles. K.D. developed eNpHR. M.P., S.M-S., and J.A.S. diagnosed and screened the records of RP patients. M.S., M.B., and P.H. made the Cnga3-/-, Rho-/- mice. B.R. designed experiments and wrote the paper.